

# A Novel Scheme to Improve the Stability of Conventional-Concentration Electrolyte at High Voltage

Jing-Jing Zhang,<sup>[a]</sup> Jie Wang,<sup>[a]</sup> Shu-Min Wu,<sup>[a]</sup> Peng Wang,<sup>[a]</sup> Jin-Long Sun,<sup>[a]</sup> Dong-Ni Zhao,<sup>[a, b]</sup> Li-Juan Zhang,<sup>[c]</sup> Li-Ping Mao,<sup>[a]</sup> Lei Niu,<sup>[a]</sup> and Xiao-Ling Cui<sup>\*[a, b]</sup>

It is well-known that conventional-concentration electrolytes (CCEs) will undergo serious oxidative decomposition in high-voltage lithium-ion batteries, while high-concentration electrolytes (HCEs) have good oxidation stability. However, HCEs are difficult to scale-up for industrial applications due to their high viscosity and cost. Herein, based on the anti-oxidation mechanism of HCE, a novel scheme to improve the stability of CCE at high voltage was proposed. By means of magnetron sputtering

LiF on  $\text{LiNi}_{0.5}\text{Mn}_{1.5}\text{O}_4$  surface and introducing  $\text{LiPO}_2\text{F}_2$  additive, a stable cathode electrolyte interphase (CEI) film is constructed in CCE. AFM results show that the constructed CEI film in CCE has better mechanical strength and adhesion than that formed by HCE. Moreover, the battery performance with the constructed CEI film in CCE, which affords high stability at high voltage, fast-charging kinetics, and improved cycling stability ( $135 \text{ mAh g}^{-1}$  after 200 cycles), is comparable to that with HCE.

## Introduction

As a new type of rechargeable battery, lithium-ion batteries (LIBs) play a key role in modern society. It is not only widely used in modern digital products such as mobile phones and notebook computers, but also in many fields such as new energy electric vehicles, aerospace and renewable energy storage.<sup>[1]</sup> However, with the pursuit of LIBs with higher capacity density, higher power density, longer service life, better safety performance and a wider range of suitable temperatures, existing industrial materials have been unable to meet the growing needs of the public. The cathode material is the core part of LIBs. The development of the 5 V cathode material with high discharge voltage plateau is an important way to improve the energy density and power density of LIBs.<sup>[2]</sup> The reported 5 V cathode materials with excellent comprehensive properties mainly include  $\text{LiNi}_{0.5}\text{Mn}_{1.5}\text{O}_4$  (LNMO),  $\text{LiCoPO}_4$ , and  $\text{LiNiPO}_4$ .<sup>[3]</sup> Among them,  $\text{LiNi}_{0.5}\text{Mn}_{1.5}\text{O}_4$  is of great interest due to its high operating voltage and  $\text{Li}^+$  ions fast-spreading three-dimensional channels.<sup>[4]</sup> However, owing to the excessive decomposition of common electrolytes (conventional-concentration electrolytes, CCEs) at high operating voltage, the inter-

face stability between high voltage cathode material and electrolyte is poor, and the electrochemical performance and safety performance of the battery cannot be guaranteed.<sup>[4b,5]</sup>

In recent years, high-concentration electrolytes (HCEs) have been found to exhibit excellent electrochemical properties in high-voltage LIBs with LNMO as the cathode material due to the generation of LiF-rich CEI film, and this conclusion has been widely accepted.<sup>[3,6]</sup> However, how about the composition and mechanical properties of a stable CEI film at high voltage? Is it really just for the reason of LiF function? There is no consensus on these questions. Recently, our group has made a breakthrough in the research on the mechanism of the stabilization of HCEs, that is, the real mechanism of HCEs showing better antioxidation at high voltage was not LiF, but the result of the interaction between LiF and the soluble decomposition product  $\text{LiPO}_2\text{F}_2$  (LiDFP).<sup>[7]</sup> However, considering the practicality of electrolytes, HCEs are difficult to use in industrial applications on account of their high viscosity (long time to be fully soaked for electrode, separator and electrolyte) and high cost.<sup>[8]</sup> Therefore, how to effectively utilize the antioxidation mechanism of HCEs at high voltage to improve the battery performance with CCEs needs to be further explored.

At present, many studies have focused on the generation of LiF by introducing co-solvents, diluents and additives with fluorine-rich (F-rich).<sup>[9]</sup> But the F-rich solvents or additives are unfortunately not only difficult to prepare, but expensive and environmentally unfriendly.<sup>[10]</sup> Inspired by the aforementioned complementarity, in this work, we construct a CEI film in the conventional-concentration electrolyte by artificial sputtering of nanoscale LiF layer on the LNMO electrode surface and introducing the electrolyte additive of LiDFP (soluble product). Systematically, we performed SEM, TEM, AFM and XPS depth profiling by an  $\text{Ar}^+$  sputtering on the CEI film with different cells to probe the characteristics (composition, morphology, and mechanical property), aiming to compare the similarities and differences between the constructed CEI film in CCE and

[a] J.-J. Zhang, Dr. J. Wang, S.-M. Wu, Dr. P. Wang, J.-L. Sun, Dr. D.-N. Zhao, Prof. L.-P. Mao, Dr. L. Niu, Prof. X.-L. Cui

School of Petrochemical Technology

Lanzhou University of Technology

730050 Lanzhou, P. R. China

E-mail: xlcuilw@163.com

[b] Dr. D.-N. Zhao, Prof. X.-L. Cui

Key Laboratory of Low Carbon Energy and Chemical Engineering of Gansu Province

730050 Lanzhou, P. R. China

[c] Prof. L.-J. Zhang

School of Chemistry and Chemical Engineering

Qinghai Minzu University

810007 Xining, P. R. China

 Supporting information for this article is available on the WWW under <https://doi.org/10.1002/batt.202200329>

that formed by HCE. The results suggest that the morphology and mechanical properties of the constructed CEI film are improved compared with those of the CEI film formed by HCE and CCE. As expected, the cell with constructed CEI film also exhibits distinguished electrochemical performance than that with HCE. More importantly, the magnetron sputtering combined with electrochemistry methods constructs the stable CEI film, which can apply the conventional-concentration electrolyte (CCE) to high-voltage LIBs, saving a great deal of cost and being prone to industrialization.

## Results and Discussion

### The remarkably poor cell performance with CCE in contrast to HCE

As shown in Figure 1(a and b), it is observed that the cell with CCE (LNMO|1 M|Li) shows remarkably poor rate performance, cycling performance and coulombic efficiency at high voltage compared with the cell with HCE (LNMO|5.5 M|Li). Thereinto, the specific capacity of LNMO|5.5 M|Li cell is 17 mAh g<sup>-1</sup> higher than that of LNMO|1 M|Li at 2 C, mainly due to the CEI film formed by HCE at high voltage, which can effectively eliminate the disadvantages of high viscosity and low conductivity of HCE. In addition, the capacity retentions of LNMO|1 M|Li at 0.5 C is only 96.8%, lower than 98.4% of LNMO|5.5 M|Li. EIS results of the cells after 200 cycles in Figure 1(c) and Table S1 display that the interfacial impedance ( $R_f$ ) and

charge transfer impedance ( $R_{ct}$ ) of LNMO|5.5 M|Li cell are 38.6  $\Omega$  and 41.06  $\Omega$ , respectively, 12.61  $\Omega$  and 567.94  $\Omega$  lower than that of LNMO|1 M|Li. Moreover, in comparison with LNMO|1 M|Li half-cell, LNMO|5.5 M|Li cell presents a smaller polarization voltage (Figures 1d and S1), attributing to the large amount of lithium salt inhibiting the movement of anions.<sup>[11]</sup> Therefore, these results indicate that HCE can effectively form a CEI film with low impedance and fast charge-transfer properties, thus promoting the intercalation/deintercalation behavior of Li<sup>+</sup> ions.<sup>[12]</sup> According to our previous research results, the stable CEI film in HCE is derived from the decomposition products of lithium salts LiPF<sub>6</sub> and soluble products LiDFP (LiF, Li<sub>x</sub>PO<sub>y</sub>F<sub>z</sub> and Li<sub>3</sub>PO<sub>4</sub>).<sup>[7]</sup>

The salient feature of HCE with better electrochemical stability at high voltage had invoked numerous theoretical studies to decipher the interaction mechanism of the electrolyte components. However, HCEs are difficult to realize industrial applications due to their high viscosity, which will prolong the electrode infiltration time, and high cost. Therefore, how to utilize the anti-oxidation mechanism of HCEs to improve the high-voltage stability of CCEs is a more worthy of exploration. Hence, we next construct a CEI film in the CCE by magnetron sputtering and electrochemical method (adding LiDFP additive), comparable to that in the HCE.

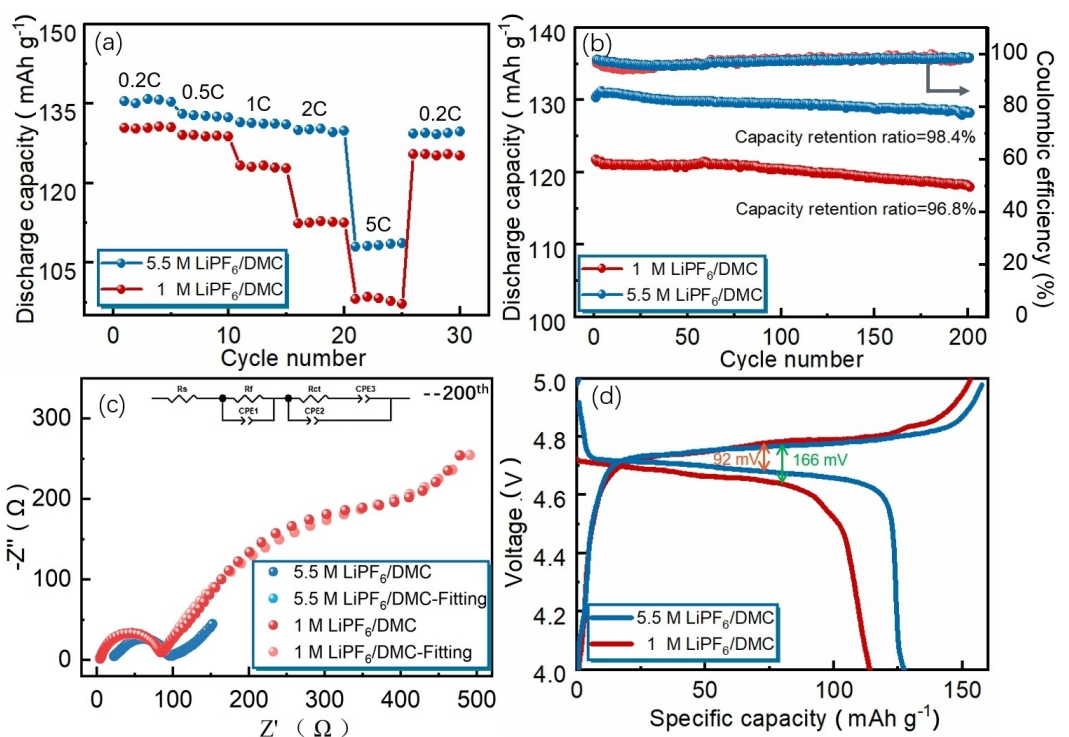


**Figure 1.** Electrochemical tests of LNMO|5.5 M|Li and LNMO|1 M|Li cells. a) Rate capability, b) cycling performance and Coulombic efficiency at 0.5 C, c) EIS plots of cycled cells (inset is equivalent circuit), d) initial voltage-capacity curves comparison.

### Construction of stable CEI film in CCE

**The characterization of LNMO-LiF.** In order to make the CEI film contain one component of the CEI film formed in HCE, LiF is artificially sputtered on the LNMO surface by magnetron sputtering (described as LNMO-LiF). SEM, EDS and TEM characterizations were preformed to verify the successful sputtering of LiF on the LNMO surface.

As shown in Figure 2(a, b), comparing with LNMO-LiF, the LNMO electrode surface is smooth and no obvious deposit sediment appears in the contact gaps. However, there are

obvious deposit sediment in the LNMO-LiF contact gaps in Figure 1(b), which suggest that LiF has been sputtered on the LNMO surface. Elemental mapping by EDS shown in Figure 2(c) displays that there is less F elements on the unmodified LNMO surface, which is mainly sourced form PVDF. On the contrary, the content of F elements on the LNMO-LiF surface increases significantly after LiF sputtering, showing a relatively uniform distribution (Figure 2d). TEM image in Figure 2(e and f) precisely identifies the presence of LiF on LNMO surface. In contrast to LNMO electrode, LNMO-LiF electrode shows obvious sediment layer at the edge of LNMO particles. The

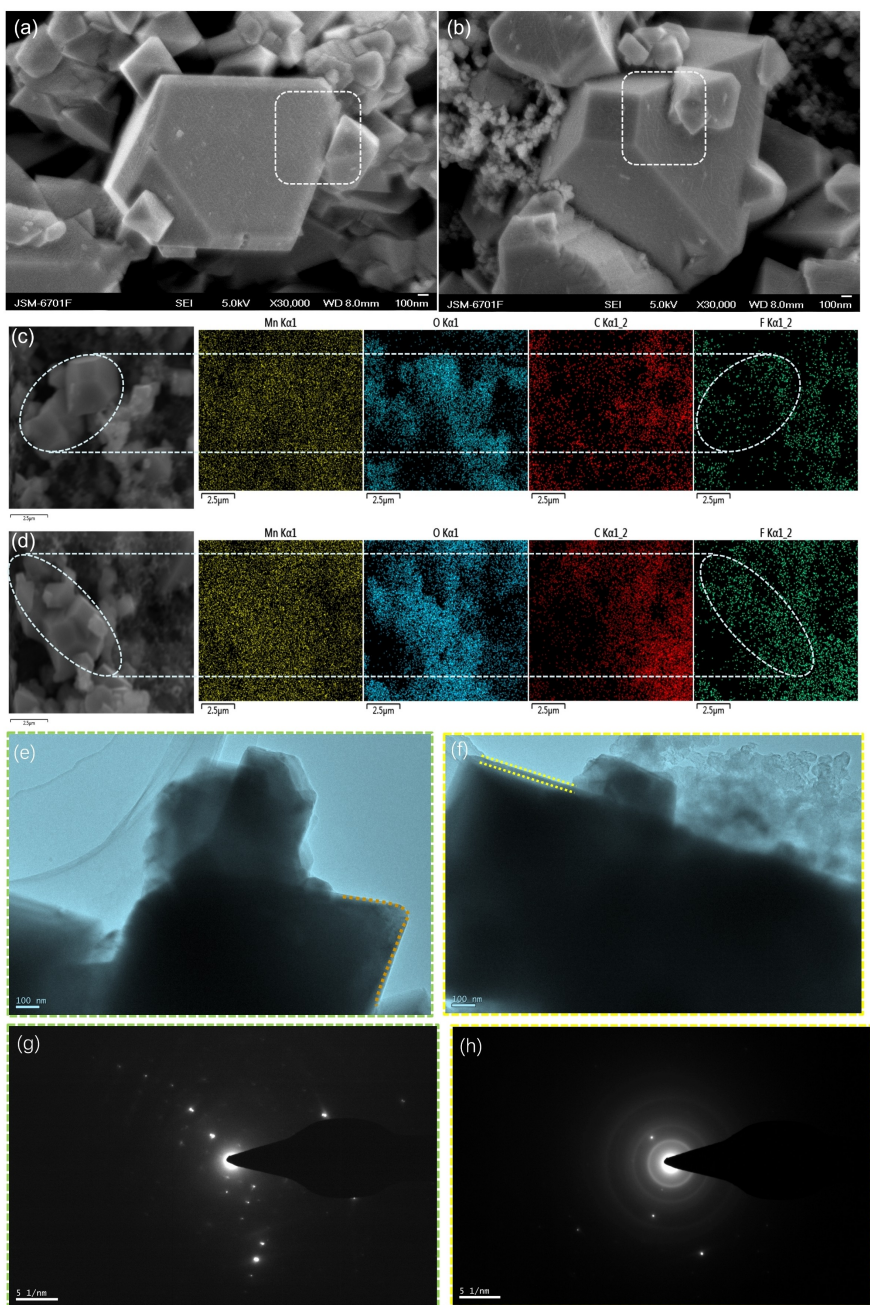


**Figure 2.** SEM, EDS and TEM characterization of LNMO and LNMO-LiF electrode materials. a), c), e), g) LNMO, b), d), f), h) LNMO-LiF.

corresponding selected area electron diffraction (SAED) in Figure 2(g and h) reveal that raw material LNMO has a single crystal structure, while the sputtered LiF has a polycrystalline structure, which is consistent with the reported conclusion that LiF has a polycrystalline structure with preferred growth orientation.<sup>[13]</sup>

The sputtering of LiF on the LNMO surface successfully endows one of the most important components of the CEI film formed by HCE, greatly increasing the possibility of constructing a stable CEI film in CCE. Apart from obtaining LNMO-LiF, we chosen 1 wt% LiDFP to introduce the soluble product LiPO<sub>2</sub>F<sub>2</sub> in CCE. LiDFP is not only soluble in electrolytes, but also produces more Li<sub>x</sub>PO<sub>y</sub>F<sub>z</sub> and Li<sub>3</sub>PO<sub>4</sub>, thereby improving the ion conductivity of CEI film.

### The electrochemical performance of the constructed CEI film

Figure 3(a, b) shows the rate and cycle performance of LNMO | 5.5 M | Li, LNMO-LiF | 1 M + LiDFP | Li, LNMO-LiF | 1 M | Li, and LNMO | 1 M + LiDFP | Li cells, respectively. The results show that LNMO | 5.5 M | Li and LNMO-LiF | 1 M + LiDFP | Li have better rate performance than LNMO-LiF | 1 M | Li and LNMO | 1 M + LiDFP | Li. In particular, the specific capacity of LNMO-LiF | 1 M + LiDFP | Li is about 15 mAh g<sup>-1</sup> higher than that of LNMO-LiF | 1 M | Li and LNMO | 1 M + LiDFP | Li when the current density increases to 2 C, achieving 128 mAh g<sup>-1</sup>. The results reconfirm that adding single LiF or soluble product in CCE does not achieve the same performance of the cell with HCE. The performance of LNMO-LiF | 1 M + LiDFP | Li cell, which takes both soluble product and LiF into consideration, is almost comparable to the cell

with HCE. It is interesting to note that the electrochemical performance of LNMO | 5.5 M | Li is superior to LNMO-LiF | 1 M + LiDFP | Li within the first 30 cycles, whereas the specific capacity of LNMO-LiF | 1 M + LiDFP | Li is about 8 mAh g<sup>-1</sup> higher than LNMO | 5.5 M | Li after 30 cycles, remaining 135 mAh g<sup>-1</sup> after 200 cycles, as shown in Figure 3(b). The main reason may be the uneven distribution of LiF on the LNMO surface, resulting in side reactions at electrode/electrolyte interface in the early cycling stages for CCE. But for HCE, the more uniform CEI film with excellent high-voltage tolerance is formed by the oxidation product LiF and the decomposition products of soluble product LiPO<sub>2</sub>F<sub>2</sub>, which are derived from continuous decomposing of more PF<sub>6</sub><sup>-</sup>. To further demonstrate the presumption, the leakage current test was carried out for LNMO | 5.5 M | Li and LNMO-LiF | 1 M + LiDFP | Li, the result is shown in Figure 3(c, d). LNMO-LiF | 1 M + LiDFP | Li has higher leakage current compared with LNMO | 5.5 M | Li, verifying that the constructed CEI film is unstable in the initial charge, and there are many surface side reactions. Besides, the specific capacity of the cell with individual LiF or LiPO<sub>2</sub>F<sub>2</sub> is lower than that of the cell with HCE in 200 cycles.

In order to explain this phenomenon, PRIs-EIS was used to monitor the electrochemical impedance of each cell in situ during the first film formation. Figure 4 shows the vertical view of Nyquist plots and 3D bode-phase graphs from PRIs-EIS with different cells. As shown in Figure 4(a1–c1), the different colors represent the range of d(-Z')/d(Z'). Among them, Z'' and Z' are the real axis and imaginary axis of EIS (such as Figure 1c).<sup>[14]</sup> The d(-Z')/d(Z') represents the slope of the tangent line at the specified frequency, while the color change from blue to red is a semicircle.

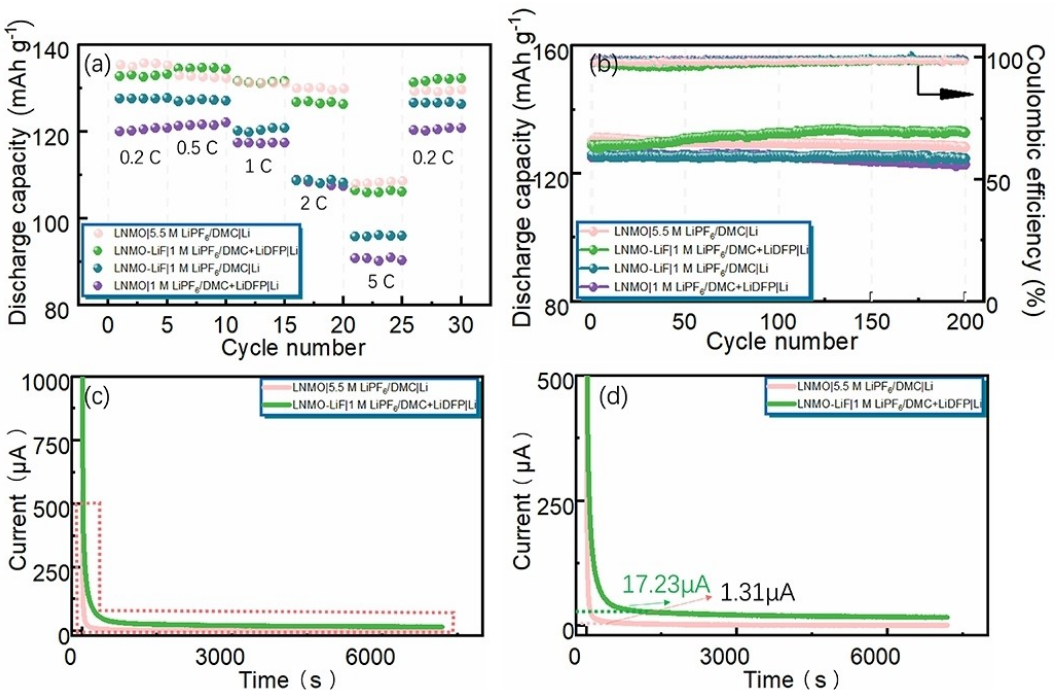
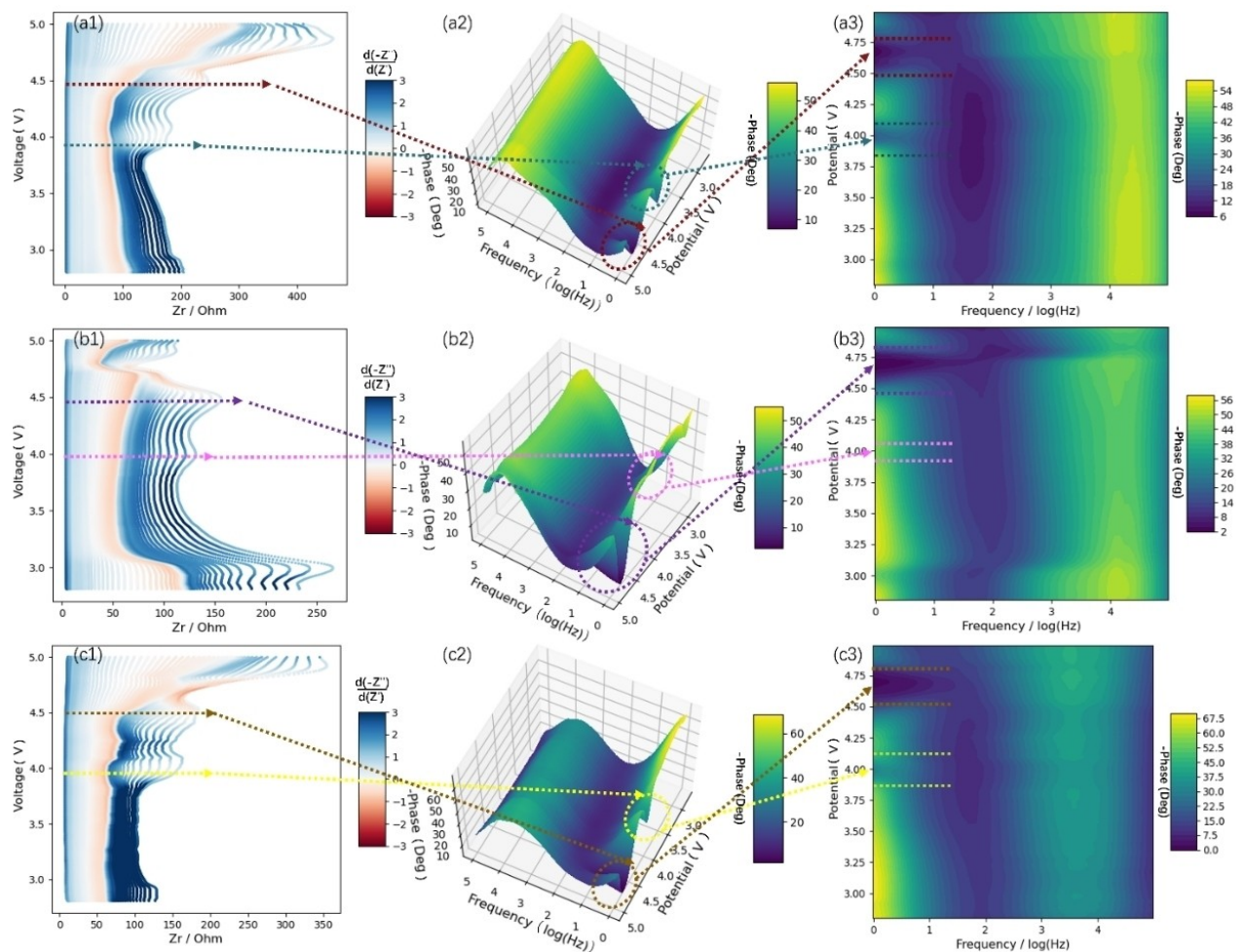


Figure 3. Electrochemical testing of different electrolyte cells. a) Rate capability, b) cycle performance, and c), d) Constant potential timing current test curve and partial enlarged drawing (Leakage Current).



**Figure 4.** The PRIs-EIS diagrams of different cells (vertical view of the Nyquist plot and 3D bode-phase graphs). a1–a3) LNMO-LiF | 1 M | Li, b1–b3) LNMO | 1 M + LiDFP | Li, c1–c3) LNMO-LiF | 1 M + LiDFP | Li.

As shown in Figure 4(a2–c2) and Figure 4(a3–c3), a trough represents a time constant, which means that the vertical view of the Nyquist plots will appear a semicircle.<sup>[15]</sup> From the comparison, we find that the initial voltage for LNMO-LiF | 1 M + LiDFP | Li cell to form the second time constant is at 4.52 V, whereas LNMO-LiF | 1 M | Li and LNMO | 1 M + LiDFP | Li cells are at 4.48 and 4.43 V, respectively. The results show that the electrolyte tolerance of cell containing both LiF and additives is improved. What's more, we find that the LNMO-LiF | 1 M + LiDFP | Li cell has lower interfacial impedance and charge transfer impedance than LNMO-LiF | 1 M | Li and LNMO | 1 M + LiDFP | Li (Table 1).

In addition, LSV was used to further prove that full use of the anti-oxidation mechanism of HCE can improve the toler-

ance of CCE at high voltage. LSV curves show that adding single LiF or LiDFP, the oxidation current of the corresponding cells increases sharply when the voltage is greater than 4.6 V, while the lower slope of LNMO-LiF | 1 M + LiDFP | Li represents its oxidation stability is obviously improved. (Figure S2). Besides, the calculation results of diffusion coefficient of  $\text{Li}^+$ -ion ( $D_{\text{Li}^+}$ ) from CV curves with different sweep speed prove that the constructed CEI film in CCE effectively promote the reaction kinetics of electrode materials due to the effect of LiDFP (Figure S3, Table S2). This also shows that the advantage of HCE at high voltage is the result of the combination of LiF and the decomposition products of soluble product  $\text{LiPO}_2\text{F}_2$ , rather than just the role of LiF as reported in the literatures.<sup>[11b,12,16]</sup>

#### Chemical composition and mechanical properties of the constructed CEI

From what has been discussed above, it may reasonably arrive at the conclusion that the electrochemical performance of LNMO-LiF | 1 M + LiDFP | Li is better than that of LNMO-LiF | 1 M | Li and LNMO | 1 M + LiDFP | Li, and the cycle and rate perform-

**Table 1.** Fitting results of electrochemical impedance spectroscopy of different cells after initial charge.

Cells	$R_s$ [ $\Omega$ ]	$R_f$ [ $\Omega$ ]	$R_{ct}$ [ $\Omega$ ]
LNMO-LiF   1 M   Li	6.899	94.47	49.16
LNMO   1 M + LiDFP   Li	4.358	157.5	490.5
LNMO-LiF   1 M + LiDFP   Li	4.035	69.01	45.01

ance can even be comparable to LNMO|5.5 M|Li. Therefore, AFM combined with SEM were carried out to gain insight into the mechanic properties and morphology of the constructed CEI film in CCE and that formed by HCE.

Figure 5(a–c) is the SEM characterization of LNMO|1 M|Li, LNMO|5.5 M|Li, and LNMO-LiF|1 M+LiDFP|Li cells after 200 cycles, respectively. Figure 5(a) shows that more particles obviously exist on the LNMO surface in the cell with unmodified CCE, and the CEI film is thick and uneven, which is related to the oxidative decomposition of DMC.<sup>[17]</sup> In the cell with HCE, less particles are observed, and the CEI film is uniform and dense (Figure 5b), which is the main reason why the electrochemical performance of LNMO|5.5 M|Li is superior to that of LNMO|1 M|Li. In contrast to HCE, the constructed CEI film in modified CCE is not only smooth and dense, but also has no particle attachment (Figure 5c).

In order to further probe the surface topography clearly, the electrode morphologies of LNMO|1 M|Li, LNMO|5.5 M|Li and LNMO-LiF|1 M+LiDFP|Li were characterized by AFM, as shown in Figure 6. LNMO|1 M|Li shows a more evenly distributed compared with LNMO|5.5 M|Li and LNMO-LiF|1 M+LiDFP|Li, which is mainly due to the fact that more particles in the generated CEI film wrap the cathode material and the substrate is relatively flat. However, LNMO|5.5 M|Li and LNMO-LiF|1 M+LiDFP|Li exhibit similar morphology and uneven surface distribution (Figure 6b1–c2). Combined with SEM results in Figure 5(b and c), the rugged surface morphology is mainly caused by the thin CEI film and a small number of attached particles.

The mechanical properties of CEI films were also measured by AFM. As shown in Figure 7, both the constructed CEI film in CCE and the CEI formed by HCE show higher Young's modulus than the generated CEI in CCE in the range of 2.0–8.0 GPa. Among them, the average Young's modulus of the CEI film formed in the LNMO|1 M|Li is 1.8 GPa. When the salt

concentration increases to 5.5 M, the average Young's modulus of CEI film increases to 2.203 GPa. Importantly, the average Young's modulus of the constructed CEI film in LNMO-LiF|1 M+LiDFP|Li is 2.315 GPa. The results show that LNMO-LiF|1 M+LiDFP|Li has higher mechanical strength, which is favorable to the stability of the cells at high operating voltage. This is consistent with the literature report that LiF can enhance the mechanical strength of interface films.<sup>[18]</sup>

Besides, according to Figure 7(a2–c2), it is found that the adhesion of generated CEI film in CCE (the average adhesion is 8.936 nN) is significantly smaller than that formed by HCE (the average adhesion is 37.081 nN) and the constructed CEI film (the average adhesion is 44.851 nN) in the range of 20.0–200 nN. This result means that the electrode/electrolyte side reaction will continue to occur in the charging and discharging process of LNMO|1 M|Li, resulting in thick and porous CEI film, which is macroscopically manifested as the capacity fading. By contrast, the adhesion of the constructed CEI film is not only significantly higher than the generated CEI in CCE, but also higher than that formed CEI in HCE. This further proves that the CEI film constructed by combining artificial and electrochemical methods can be comparable to that formed by HCE. It solves the problem of poor mechanical strength of CCE, moreover ensures good contact between electrode and CEI film, which provides support for stable operation of LIBs at high voltage.<sup>[19]</sup>

To better understand the chemical composition of CEI films after cycling, the surface of these cycled LNMO electrodes were further investigated by XPS analysis. As shown in Figure 8(a1–a4, e1–e4, and i1–i4), C 1s and O 1s peaks at 284.8 eV, 287.6 and 534.2 eV, 288.8 and 533.1 eV, and 290.1 eV correspond to C–C, C=O and PVDF respectively, which are attributed to acetylene black, the decomposition products of carbonate solvent and PVDF.<sup>[7,20]</sup> O 1s peaks at 530.8 eV and 531.8 eV correspond to Li–O and H–O, which belong to alkoxy lithium (ROLi) and RCOOLi respectively.<sup>[12,21]</sup> F 1s and P 2p peak at 688.6 eV and 134.5 eV corresponding to Li<sub>x</sub>PO<sub>y</sub>F<sub>z</sub>, F 1s located at 686.5 eV belongs to LiF.<sup>[22]</sup> P 2p peaks at 133.2 eV and 135.2 eV correspond to Li<sub>3</sub>PO<sub>4</sub> and Li<sub>x</sub>PO<sub>y</sub>F<sub>z</sub>, respectively.<sup>[7,23]</sup> By comparing the LNMO|1 M|Li and LNMO|5.5 M|Li cells, it is found that the contents of decomposition products of carbonate solvent in CEI film formed by HCE is smaller than the generated CEI film in CCE, while the content of Li<sub>x</sub>PO<sub>y</sub>F<sub>z</sub>, LiF, Li<sub>3</sub>PO<sub>4</sub>, Li<sub>x</sub>PO<sub>y</sub>F<sub>z</sub> is higher (Figure 8a1–a4, e1–e4). It means that the chemical composition of the CEI film formed by LNMO|5.5 M|Li after 200 cycles is still dominated by the decomposition product of LiPF<sub>6</sub>. On the contrary, although both LNMO-LiF|1 M+LiDFP|Li and LNMO|1 M|Li are the cells with CCE, the chemical composition of the CEI film of the former is similar with that of the CEI film formed by HCE, and the content of Li<sub>3</sub>PO<sub>4</sub> is higher than that of CEI film formed by HCE, accounting for why the cycle performance of LNMO-LiF|1 M+LiDFP|Li is better than LNMO|5.5 M|Li.

To further characterize the chemical composition of the CEI film, XPS with an Ar<sup>+</sup> sputtering depth profiling was performed shown in Figure 8. With the increase of sputtering time (1 nm/s) to 30 s, the content of C–O and C=O (O 1s) in the three cells decrease gradually and the content of LiF gradually increase,

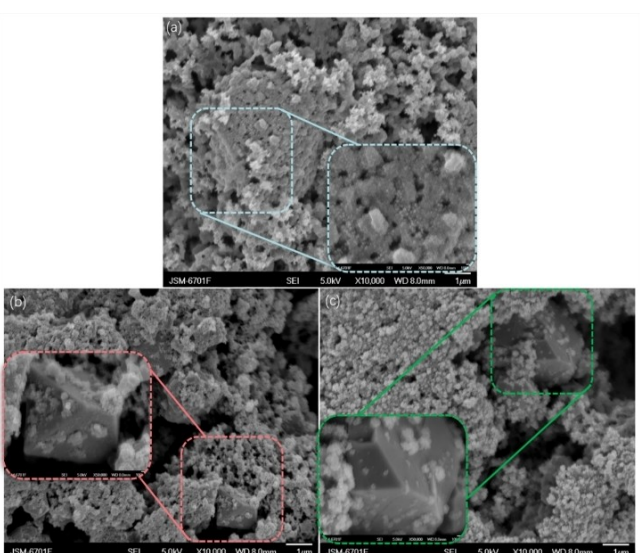
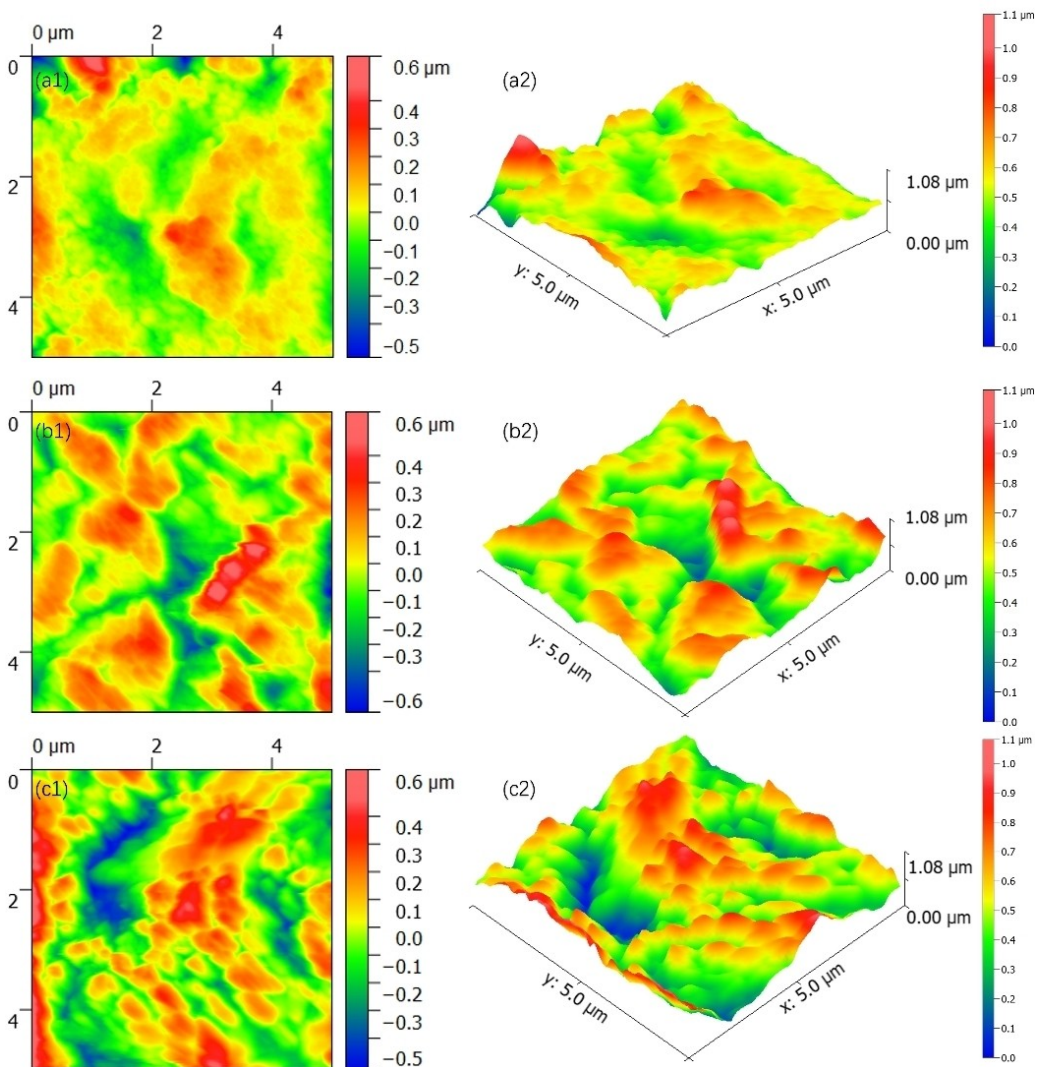


Figure 5. The SEM of (a) LNMO|1 M|Li, (b) LNMO|5.5 M|Li, (c) and LNMO-LiF|1 M+LiDFP|Li cells after 200 cycles. The scale bars are 1 μm.



**Figure 6.** The surface morphology ( $5 \times 5 \mu\text{m}^2$ ) and 3D topographical AFM image of a1) and a2) LNMO | 1 M | Li, b1) and b2) LNMO | 5.5 M | Li, c1) and c2) and LNMO-LiF | 1 M + LiDFP | Li cells after 200 cycles.

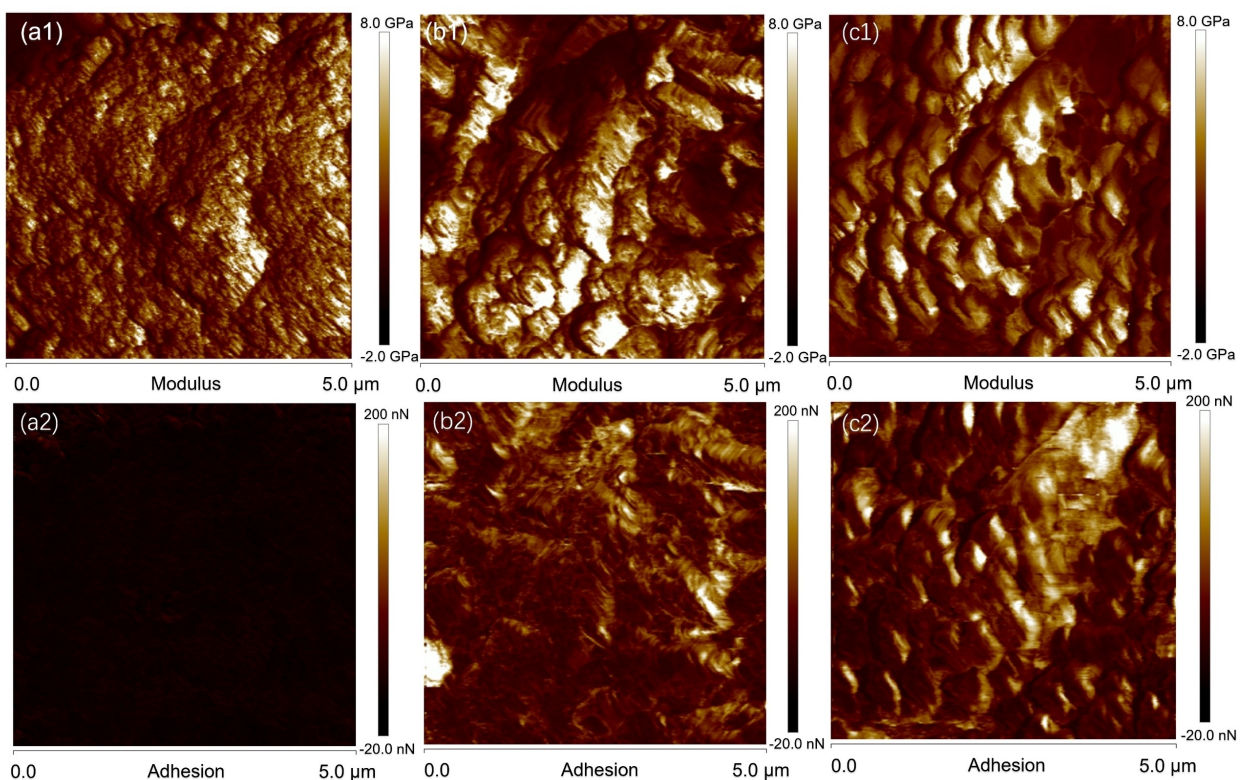
which is agreement with the previous reports that inorganic and organic products are generally distributed in the inner and outer layers of CEI film, respectively.<sup>[24]</sup> When the sputtering time increases to 45 s, the contents of LiF,  $\text{Li}_x\text{PO}_y\text{F}_z$  and  $\text{Li}_3\text{PO}_4$  in the constructed CEI in CCE, remain basically unchanged. Among them,  $\text{Li}_3\text{PO}_4$  in the constructed CEI film is mainly the decomposition product of additive  $\text{LiPO}_2\text{F}_2$ .

Figure 9 is the mechanism diagram designed for this study based on our previous research results, that of, the sputtering LiF increases the content of LiF in the constructed CEI film in CCE, while the additive replaces the role of soluble product in high-concentration electrolyte and participates in oxidative decomposition to increase the content of  $\text{Li}_x\text{PO}_y\text{F}_z$  and  $\text{Li}_3\text{PO}_4$ .

It follows that the method of the constructed CEI film in CCE by combining magnetron sputtering LiF on  $\text{LiNi}_{0.5}\text{Mn}_{1.5}\text{O}_4$  surface and introducing  $\text{LiPO}_2\text{F}_2$  can successfully solve the problem of high cost of HCE. Especially, the stability of the constructed CEI film in high-voltage LIBs can be improved completely.

## Conclusion

In our previous study, we found that compared with CCE, HCE had better anti-oxidation at high voltage mainly due to the formation of CEI film composed of LiF,  $\text{Li}_x\text{PO}_y\text{F}_z$  and  $\text{Li}_3\text{PO}_4$ . However, the high cost and viscosity of HCE seriously limit its industrial application. Therefore, this study makes full use of the anti-oxidation mechanism of HCE to construct a CEI film in CCE by combining artificial and electrochemical methods, so as to improve the tolerance of CCE at high operating voltage. The electrochemical performance and characterizations of SEM, TEM, AFM, and XPS with  $\text{Ar}^+$  sputtering depth profiles for CEI films showed that the cell containing the constructed CEI film exhibits better electrochemical performance than the cell with HCE. Moreover, the mechanical strength of the constructed CEI film and its contact effect with electrode are comparable to that of the CEI film formed by HCE. This study can not only extend the application of CCE to high-voltage LIBs, but also provide research directions for other stable interface designs. In



**Figure 7.** The AFM image of Young's modulus and adhesion of a1) and a2) LNMO|1 M|Li, b1) and b2) LNMO|5.5 M|Li, c1) and c2) LNMO-LiF|1 M+LiDFP|Li cells after 200 cycles.

addition, the optimization of the LiF magnetron sputtering thickness and the amount of additive needs to further studied in the follow-up research to provide a clearer guidance for stabilizing the high-voltage cathode/electrolyte interface.

## Experimental Section

**Materials:** All of the electrolytes (Guangdong Candlelight New Energy Technology Co., Ltd.) including 1 M LiPF<sub>6</sub>/DMC, 5.5 M LiPF<sub>6</sub>/DMC, and 1 M LiPF<sub>6</sub>/DMC + 1% LiDFP were battery-grade purities. LiNi<sub>0.5</sub>Mn<sub>1.5</sub>O<sub>4</sub> was provided by Shenzhen Baxter New Energy Materials Co., Ltd.

**Preparation of electrode:** The LiNi<sub>0.5</sub>Mn<sub>1.5</sub>O<sub>4</sub> was mixed with conductive carbon black and polyvinylidene fluoride binder (PVDF) in a mass ratio of 80:10:10 to make a uniform slurry with N-methyl-2-pyrrolidinone (NMP) solvent, which was then coated on aluminum foil and vacuum dried for 12 h at 110 °C. Finally, 14 mm discs were obtained from the dried pieces and the loading amount was around 1.2–2.0 mg cm<sup>-2</sup>. Besides, the prepared LNMO electrode was magnetron sputtered with LiF to obtain LNMO-LiF electrode. The LiF layer, a thick (~10 nm) calibration layer, was

deposited using RF magnetron sputtering (JGP450B, SKY Technology Development Co., Ltd).

**Battery assembly:** The CR2025 cells were assembled in a glove box (O<sub>2</sub> and H<sub>2</sub>O < 0.1 ppm). Its components mainly include electrode (the diameter is 14 mm), lithium plate (the diameter is 15.7 mm), separator (PP/PE/PP) and electrolyte. The abbreviations of cells corresponding to different electrodes and electrolytes is shown in Table 2.

**Electrochemical measurements:** The electrochemical performances of the cells were tested on the LAND-CT2001A (Wuhan, China) with the voltage range 3.5–5 V. In addition, DH7000 (Jiangsu Dong Hua, China) and CHI660E (Shanghai Chenhua, China) Electrochemical Workstations were used to measure the electrochemical impedance spectroscopy (EIS), cyclic voltammetry (CV), potential-resolved *in situ* electrochemical impedance spectroscopy (PRIs-EIS), linear sweep voltammetry (LSV), and chronoamperometry (CA). The amplitude of EIS is 5 mV and the frequency is 10<sup>5</sup>–0.1 Hz. The CV curves of the cells were completed at the potential range of 3.5–5 V with a scanning rate of 0.1, 0.3, 0.5, 0.7 and 1 mVs<sup>-1</sup>. The chronoamperometry was performed with a polarized voltage of 10 mV over 2 hours.

**The CEI film characterization:** Scanning electron microscopy (SEM, JSM-6510), Transmission electron microscopy (TEM, JEM-2100),

**Table 2.** The abbreviations of cells corresponding to different electrodes and electrolytes.

Electrodes	Electrolytes		
	1 M LiPF <sub>6</sub> /DMC	5.5 M LiPF <sub>6</sub> /DMC	1 M LiPF <sub>6</sub> /DMC + 1% LiPO <sub>2</sub> F <sub>2</sub>
LNMO	LNMO 1 M Li	LNMO 5.5 M Li	LNMO 1 M+LiDFP Li
LNMO-LiF	LNMO-LiF 1 M Li	LNMO-LiF 5.5 M Li	LNMO-LiF 1 M+LiDFP Li

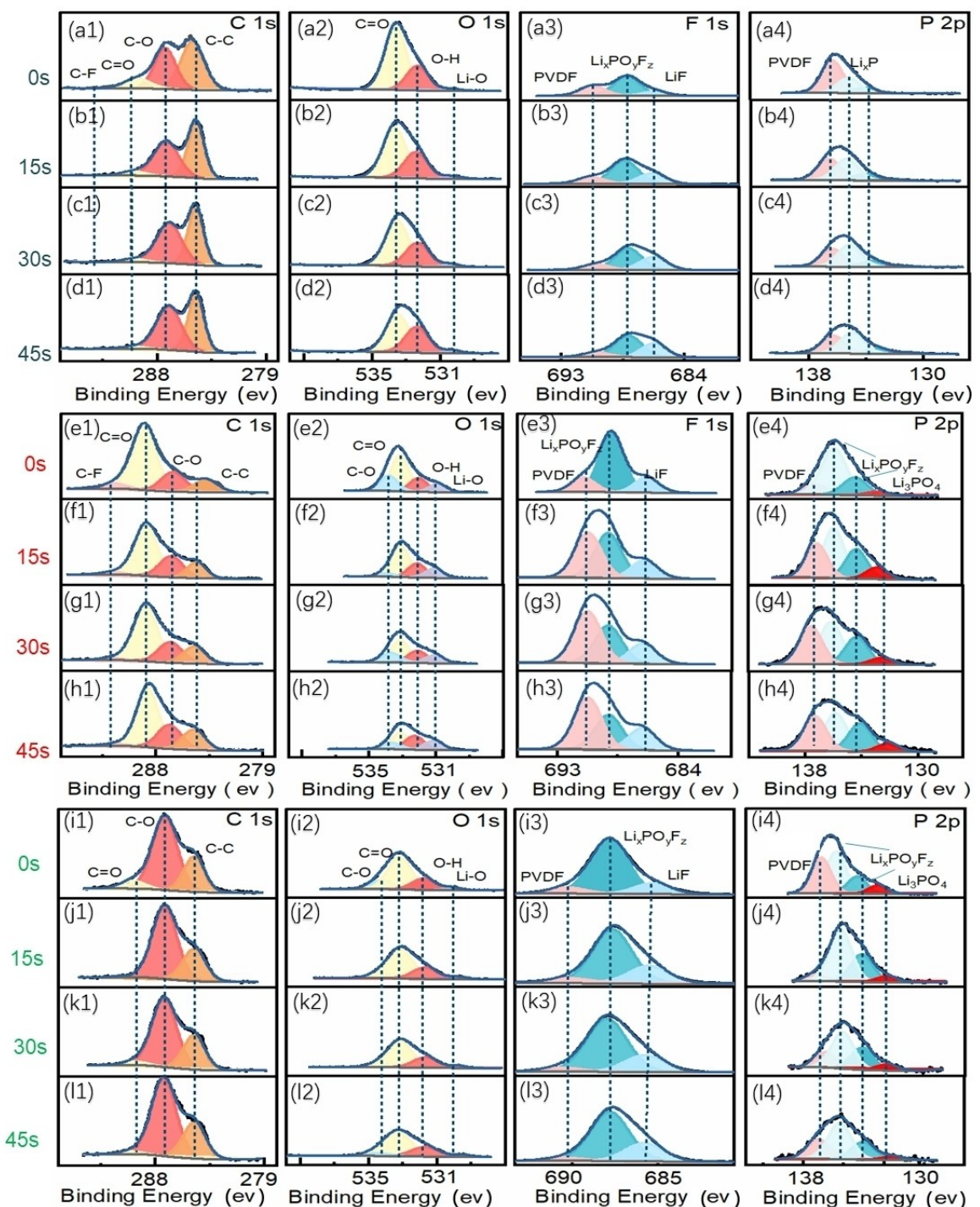


**Figure 8.** The XPS with an  $\text{Ar}^+$  sputtering depth profiling of (a1–d4)  $\text{LNMO} | 1 \text{ M} | \text{Li}$ , (e1–h4)  $\text{LNMO} | 5.5 \text{ M} | \text{Li}$ , (i1–l4) and  $\text{LNMO-LiF} | 1 \text{ M} + \text{LiDFP} | \text{Li}$  cells after 200 cycles.

Atomic Force Microscopy (AFM, Bruker Dimension ICON) and X-ray photoelectron spectroscopy (XPS, Thermo ESCALAB) were used to probe the characteristics (composition, morphology, and mechanical property) of the CEI film with different cells (all operations were done in glove box).

### Acknowledgements

This work was supported by the Major Projects of Gansu Province (18ZD2FA012), Natural Science Foundation of Gansu Province for Youths (21JR7RA254), and the program of science and technology international cooperation project of Qinghai province (No. 2022-HZ-809).

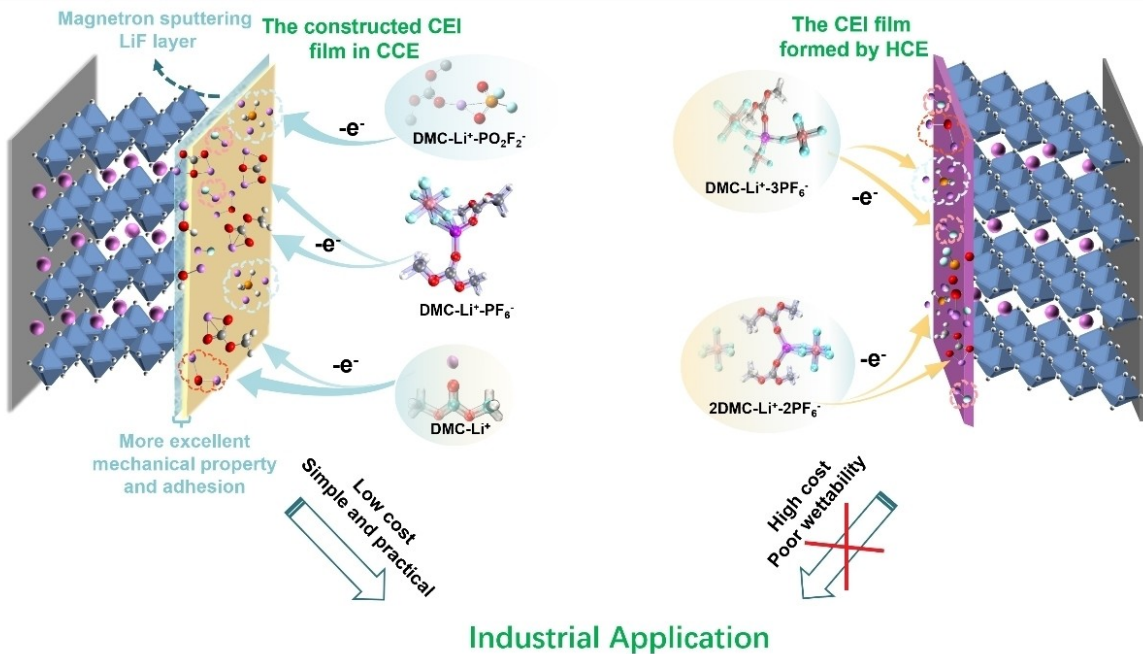


Figure 9. Mechanism diagram of CEI film constructed by artificial and electrochemical methods.

## Conflict of Interest

The authors declare no conflict of interest.

## Data Availability Statement

The data that support the findings of this study are available from the corresponding author upon reasonable request.

**Keywords:** anti-oxidation • cathode-electrolyte interphase • conventional-concentration electrolyte • high-concentration electrolyte • high voltage

- [1] a) X. Xu, K. Lin, D. Zhou, Q. Liu, X. Qin, S. Wang, S. He, F. Kang, B. Li, G. Wang, *Chem.* **2020**, *6*, 902–918; b) K. Qin, K. Holguin, M. Mohammadiroudbari, J. Huang, E. Y. S. Kim, R. Hall, C. Luo, *Adv. Funct. Mater.* **2021**, *31*, 2009694.
- [2] S. Tao, F. Kong, C. Wu, X. Su, T. Xiang, S. Chen, H. Hou, L. Zhang, Y. Fang, Z. Wang, W. Chu, B. Qian, L. Song, *J. Alloys Compd.* **2017**, *705*, 413–419.
- [3] T. Doi, R. Masuhara, M. Hashinokuchi, Y. Shimizu, M. Inaba, *Electrochim. Acta* **2016**, *209*, 219–224.
- [4] a) L. Wei, J. Tao, Y. Yang, X. Fan, X. Ran, J. Li, Y. Lin, Z. Huang, *Chem. Eng. J.* **2020**, *384*, 123268; b) Z. Zou, H. Xu, H. Zhang, Y. Tang, G. Cui, *ACS Appl. Mater. Interfaces* **2020**, *12*, 21368–21385.
- [5] D. Zhao, S. Li, *Front. Chem.* **2020**, *8*, 821.
- [6] a) J. Wang, Y. Yamada, K. Sodeyama, C. H. Chiang, Y. Tateyama, A. Yamada, *Nat. Commun.* **2016**, *7*, 12032; b) T. Doi, Y. Shimizu, M. Hashinokuchi, M. Inaba, *ChemElectroChem* **2017**, *4*, 2398–2403.
- [7] X. Cui, J. Zhang, J. Wang, P. Wang, J. Sun, H. Dong, D. Zhao, C. Li, S. Wen, S. L. ACS Appl. Mater. Interfaces **2021**, *13*, 59580–59590.
- [8] a) J. Zheng, J. A. Lochala, A. Kwok, Z. D. Deng, J. Xiao, *Adv. Sci. Mater.* **2017**, *4*, 1700032; b) Y. Yamada, J. Wang, S. Ko, E. Watanabe, A. Yamada, *Nat. Energy* **2019**, *4*, 269–280.

- [9] a) L. Dong, Y. Liu, D. Chen, Y. Han, Y. Ji, J. Liu, B. Yuan, Y. Dong, Q. Li, S. Zhou, S. Zhong, Y. Liang, M. Yang, C. Yang, W. He, *Energy Storage Mater.* **2022**, *44*, 527–536; b) L. Xia, H. Miao, C. Zhang, G. Z. Chen, J. Yuan, *Energy Storage Mater.* **2021**, *38*, 542–570; c) Z. Cao, X. Zheng, Q. Qu, Y. Huang, H. Zheng, *Adv. Mater.* **2021**, *33*, e2103178; d) Y. Lee, T. K. Lee, S. Kim, J. Lee, Y. Ahn, K. Kim, H. Ma, G. Park, S.-M. Lee, S. K. Kwak, N.-S. Choi, *Nano Energy* **2020**, *67*, 104309.
- [10] S. Yuan, S. Weng, F. Wang, X. Dong, Y. Wang, Z. Wang, C. Shen, J. L. Bao, X. Wang, Y. Xia, *Nano Energy* **2021**, *83*, 104309.
- [11] a) X. Fan, L. Chen, X. Ji, T. Deng, S. Hou, J. Chen, J. Zheng, F. Wang, J. Jiang, K. Xu, C. Wang, *Chem.* **2018**, *4*, 174–185; b) J.-D. Xie, J. Patra, P. Chandra Rath, W.-J. Liu, C.-Y. Su, S.-W. Lee, C.-J. Tseng, Y. A. Gandomi, J.-K. Chang, *J. Power Sources* **2020**, *450*, 227657; c) H. Wang, J. Liu, J. He, S. Qi, M. Wu, F. Li, J. Huang, J. Ma, *eScience* **2022**. DOI: 10.1016/j.escl.2022.06.005.
- [12] S. Das, *J. Electroanal. Chem.* **2020**, *879*, 114794.
- [13] W. Huang, H. Wang, D. T. Boyle, Y. Li, Y. Cui, *ACS Energy Lett.* **2020**, *5*, 1128–1135.
- [14] P. Wang, D. Yan, C. Wang, H. Ding, H. Dong, J. Wang, S. Wu, X. Cui, C. Li, D. Zhao, S. Li, *Appl. Surf. Sci.* **2022**, *596*, 153572.
- [15] P. Wang, X. Cui, D. Zhao, D. Yan, H. Ding, H. Dong, J. Wang, S. Wu, S. Li, *J. Power Sources* **2022**, *535*, 231451.
- [16] Y. Yamada, *B. Chem. Soc. Jpn.* **2020**, *93*, 109–118.
- [17] a) S. Liu, Q. Zhang, X. Wang, M. Xu, W. Li, B. L. Lucht, *ACS Appl. Mater. Interfaces* **2020**, *12*, 33719–33728; b) S. Chen, J. Zheng, D. Mei, K. S. Han, M. H. Engelhard, W. Zhao, W. Xu, J. Liu, J. G. Zhang, *Adv. Mater.* **2018**, *30*, e1706102; c) S. Lin, H. Hua, Z. Li, J. Zhao, *ACS Appl. Mater. Interfaces* **2020**, *12*, 33710–33718.
- [18] J. Tan, J. Matz, P. Dong, J. Shen, M. Ye, *Adv. Energy Mater.* **2021**, *11*, 2100046.
- [19] Y. C. Ji, K. Yang, M. Q. Liu, S. M. Chen, X. H. Liu, B. Yang, Z. J. Wang, W. Y. Huang, Z. B. Song, S. D. Xue, Y. D. Fu, L. Y. Yang, T. S. Miller, F. Pan, *Adv. Funct. Mater.* **2021**, *31*, 2104830.
- [20] a) H. Zhao, J. Gu, Y. Gao, Q. Hou, Z. Ren, Y. Qi, K. Zhang, C. Shen, J. Zhang, K. Xie, *J. Energy Chem.* **2020**, *51*, 362–371; b) X. L. Cui, S. M. Wang, X. S. Ye, X. Q. Fan, C. K. Gao, Y. Quan, S. X. Wen, X. P. Cai, J. Huang, S. Y. Li, *Energy Storage Mater.* **2022**, *45*, 1153–1164.
- [21] a) J. Chen, X. Fan, Q. Li, H. Yang, M. R. Khoshi, Y. Xu, S. Hwang, L. Chen, X. Ji, C. Yang, H. He, C. Wang, E. Garfunkel, D. Su, O. Borodin, C. Wang, *Nat. Energy* **2020**, *5*, 386–397; b) T. D. Pham, K. K. Lee, *Small* **2021**, *17*, e2100133; c) J. Li, W. Li, Y. You, A. Manthiram, *Adv. Energy Mater.* **2018**, *8*, 1801957; d) K. Jung, T. Yim, *J. Alloys Compd.* **2020**, *834*, 155155.

- [22] a) B. Wen, Z. Deng, P.-C. Tsai, Z. W. Lebens-Higgins, L. wF. J. Piper, S. P. Ong, Y.-M. Chiang, *Nat. Energy* **2020**, *5*, 578–586; b) F. Wu, J. Y. Dong, L. Chen, L. Y. Bao, N. Li, D. Y. Cao, Y. Lu, R. X. Xue, N. Liu, L. Wei, Z. R. Wang, S. Chen, Y. F. Su, *Energy Storage Mater.* **2021**, *41*, 495–504; c) F. Li, J. Liu, J. He, Y. Hou, H. Wang, D. Wu, J. Huang, J. Ma, *Angew. Chem. Int. Ed.* **2022**, *61*, e202205091.
- [23] a) K. Zhang, Y. Tian, C. Wei, Y. An, J. Feng, *Appl. Surf. Sci.* **2021**, *553*, 149566; b) J. Wang, H. Dong, P. Wang, X.-L. Fu, N.-S. Zhang, D.-N. Zhao, S.-Y. Li, X.-L. Cui, *J. Energy Chem.* **2022**, *67*, 55–64.
- [24] a) E. Peled, S. Menkin, *J. Electrochem. Soc.* **2017**, *164*, A1703–A1719; b) M. Nie, B. L. Lucht, *J. Electrochem. Soc.* **2014**, *161*, A1001; c) Y. Chu, Y. Shen, F. Guo, X. Zhao, Q. Dong, Q. Zhang, W. Li, H. Chen, Z. Luo, L. Chen, *Electrochem. Energy Rev.* **2019**, *3*, 187–219.

Manuscript received: July 21, 2022  
Revised manuscript received: September 27, 2022  
Accepted manuscript online: September 29, 2022  
Version of record online: November 3, 2022